1 **Developmental dynamics of voltage-gated sodium channel isoform expression in the human**
2 **and mouse neocortex**
3
4 Lindsay Liang[1], Siavash Fazel Darbandi[1], Sirisha Pochareddy[2], Forrest O. Gulden[2], Michael C.
5 Gilson[1], Brooke K. Sheppard[1], Atehsa Sahagun[3], Joon-Yong An[4], Donna M. Werling[5], John L.R.
6 Rubenstein[1], Nenad Šestan[2,6,7,8,9], Kevin J. Bender[3], and Stephan J. Sanders[1,10,11,†]
7
8 [1]Department of Psychiatry and Behavioral Sciences, University of California, San Francisco, San
9 Francisco, CA 94158.
10 [2]Department of Neuroscience and Kavli Institute for Neuroscience, Yale School of Medicine,
11 New Haven, CT 06510, USA.
12 [3]Department of Neurology, University of California, San Francisco, San Francisco, CA 94158,
13 USA.
14 [4]School of Biosystem and Biomedical Science, College of Health Science, Korea University,
15 Seoul, 02841, Republic of Korea.
16 [5]Laboratory of Genetics, University of Wisconsin-Madison, Madison, WI 53706, USA.
17 [6]Program in Cellular Neuroscience, Neurodegeneration, and Repair and Yale Child Study Center,
18 Yale School of Medicine, New Haven, CT 06510, USA.
19 [7]Department of Psychiatry, Yale University School of Medicine, New Haven, CT 06520, USA.
20 [8]Department of Genetics, Yale University School of Medicine, New Haven, CT 06520, USA.
21 [9]Department of Comparative Medicine, Program in Integrative Cell Signaling and Neurobiology
22 of Metabolism, Yale School of Medicine, New Haven, CT 06510, USA.
23 [10]Institute for Human Genetics, University of California, San Francisco, San Francisco, CA 94158,
24 USA.
25 [11]Bakar Computational Health Sciences Institute, University of California, San Francisco, San
26 Francisco, CA 94158, USA.
27
28 [†]Please address correspondence to: stephan.sanders@ucsf.edu (S.J.S.)
29
30

31 **Abstract**

32

33 **Objective:** Genetic variants in the voltage-gated sodium channels *SCN1A*, *SCN2A*, *SCN3A*, and
34 *SCN8A* are leading causes of epilepsy, developmental delay, and autism spectrum disorder. The
35 mRNA splicing patterns of all four genes vary across development in the rodent brain, including
36 mutually exclusive copies of the fifth protein-coding exon detected in the neonate (5N) and
37 adult (5A). A second pair of mutually exclusive exons is reported in *SCN8A* only (18N and 18A).
38 We aimed to quantify the expression of individual exons in the developing human neocortex.
39 **Methods:** RNA-seq data from 176 human dorsolateral prefrontal cortex samples across
40 development were analyzed to estimate exon-level expression. Developmental changes in exon
41 utilization were validated by assessing intron splicing. Exon expression was also estimated in
42 RNA-seq data from 58 developing mouse neocortical samples.
43 **Results:** In the mature human neocortex, exon 5A is consistently expressed at least 4-fold
44 higher than exon 5N in all four genes. For *SCN2A*, *SCN3A*, and *SCN8A* a synchronized 5N/5A
45 transition occurs between 24 post-conceptual weeks (2nd trimester) and six years of age. In
46 mice, the equivalent 5N/5A transition begins at or before embryonic day 15.5. In *SCN8A,* over
47 90% of transcripts in the mature human cortex include exon 18A. Early in fetal development,
48 most transcripts include 18N or skip both 18N and 18A, with a transition to 18A inclusion
49 occurring from 13 post-conceptual weeks to 6 months of age. No other protein-coding exons
50 showed comparably dynamic developmental trajectories.
51 **Significance:** Splice isoforms, which alter the biophysical properties of the encoded channels,
52 may account for some of the observed phenotypic differences across development and
53 between specific variants. Manipulation of the proportion of splicing isoforms at appropriate
54 stages of development may act as a therapeutic strategy for specific mutations or even epilepsy
55 in general.

56

60

1. Introduction

Genetic variation in the genes *SCN1A*, *SCN2A*, *SCN3A*, and *SCN8A* are a major cause of epileptic encephalopathy (EE), autism spectrum disorder (ASD), and developmental delay.[1–3] These four homologous genes encode voltage-gated sodium channels (Na$_V$1.1, Na$_V$1.2, Na$_V$1.3, and Na$_V$1.6 respectively) that are critical for a range of functions in the central nervous system,[4] including axonal action potential initiation and propagation,[5,6] dendritic excitability,[7,8] macroscopic anatomical development,[9] and activity-dependent myelination.[10] The functional role, subcellular location, expression-level, and isoform selection of voltage-gated sodium channels vary across development and understanding this relationship is critical for understanding the etiology of the associated disorders and their therapeutic management.[7,11–19] While some isoform-level differences have been assayed in rodents and mature human brains,[20–22] the trajectories in the developing human cortex have not been described.[23]

Sodium channel genes are composed of multiple exons, which can be protein-coding (CDS for CoDing Sequence), untranslated regions (UTRs), or non-coding exons (NCEs). Differing combinations of these exons are called isoforms, which can change the amino acid sequence of the encoded proteins (proteoforms). The best-characterized isoform change across these four sodium channels are the two mutually exclusive copies of the fifth protein-coding exon.[17,24] This exon encodes part of the first domain of the Na$_V$ channel, including the end of transmembrane segment S3, most of transmembrane segment S4, and a short extracellular linker connecting these two segments. In humans, each copy of this fifth protein-coding exon is 92 nucleotides in length, encoding 30 amino acids, of which one to three amino acids vary between the two exon copies for each gene (Fig. 1B). 'A' isoforms (5A) include the ancestral and canonical copy, with an aspartic acid residue (Asp/D) encoded at position 7 of 30.[25] 'N' isoforms (5N) use the alternative copy, with an asparagine (Asn/N) residue at position 7 of 30 in *SCN1A*, *SCN2A*, and *SCN8A* and a serine residue (Ser/S) in *SCN3A*. Despite this relatively small change in protein structure, differential inclusion of 5N or 5A can have marked effects on channel function. Indeed, these splice isoforms can alter channel electrophysiological characteristics,[26,27] the functional impacts of variants associated with seizure,[23] neuronal excitability,[28] response to anti-epileptics,[21,22,26] and seizure-susceptibility.[28]

The utilization of the 5N or 5A varies across development, with 5N generally being expressed at higher levels in the neonatal period while 5A predominates in adults.[27] This switch is defined best in mouse, where the 5N:5A ratio varies by gene and brain region along with developmental stage.[20] For *Scn2a* in mouse neocortex, the 5N:5A ratio is 2:1 at birth (postnatal day 0/P0) and flips to 1:3 by P15. For both *Scn3a* and *Scn8a*, 5A predominates throughout the postnatal period with a 1:2 ratio at P0 increasing to 1:5 by P15.[20] *Scn1a* lacks a functional copy of 5N in the mouse genome. Similar developmental profiles currently have not been reported for humans beyond the of 5N/5A utilization *SCN1A* in adults, in which a 5N:5A ratio of over 1:5 was observed in the temporal cortex and hippocampus of adult surgical resections.[21,22]

In addition to the 5N/5A switch, a similar developmental shift in mutually exclusive exons has been reported for "exons 18N or 18A" in *SCN8A* only, regulated by the RNA-binding protein RBFOX1.[16,29,30] Using GENCODE human v31 gene definitions,[31] 18A maps to the 20th protein-

105   coding exon of major *SCN8A* isoforms (CDS 20, Fig. 1A), while 18N encodes the 8th and last

106   protein-coding exon (CDS 8) of a shorter eight protein-coding exon transcript

107   (ENST00000548086.3, Fig. S1). In the embryonic mouse brain, most *SCN8A* transcripts include

108   18N or skip both 18N and 18A, leading to non-functional channels, while 18A predominates in

109   the adult mouse and human brain.[16]

110

111   Here, we present data on the utilization of GENCODE-annotated protein-coding exons in four

112   seizure-associated voltage-gated sodium channels in the human and mouse neocortex across

113   development. We demonstrate a synchronized transition from 5N to 5A utilization between 24

114   post-conceptual weeks (2nd trimester) and six years-of-age across all four voltage-gated sodium

115   channels and a transition from 18N to 18A in *SCN8A* from 13 post-conceptual weeks to 6

116   months-of-age. These isoform differences can modify the function of the encoded voltage-

117   gated sodium channels, raising the potential that interventions, such as antisense

118   oligonucleotides, could be used to modify the isoform ratio as a potential therapy for disorders

119   caused by variants in sodium channel genes or epilepsy.

120

121 **2. Materials and Methods**

122

123 **2.1 Genomic data**

124 To quantify the relative proportion of protein-coding exon expression across development in

125 the human cortex, we assessed bulk tissue RNA-seq data from 176 *post mortem* dorsolateral

126 prefrontal cortex (DLPFC) samples from the BrainVar cohort.[32] The BrainVar cohort also has

127 corresponding whole-genome sequencing data that were used to derive per sample genotypes,

128 as described previously.[32] To assess corresponding patterns of exon expression in mouse cortex

129 across development, we assessed 58 samples with bulk tissue RNA-seq data in wildtype C57/B6

130 mice. Thirty-four of these were generated as controls for ongoing experiments and 24 were

131 downloaded from GEO.[33]

132

133 **2.2 Exon expression**

134 To assess exon expression in the human cortex, the 100bp paired-read RNA-seq data from

135 BrainVar were aligned to the GRCh38.p12 human genome using STAR aligner[34] and exon-level

136 read counts for GENCODE v31 human gene definitions were calculated with DEXSeq[35] and

137 normalized to counts per million (CPM).[36] Despite the similar amino acid sequence, the

138 nucleotide sequence of 5N and 5A is sufficiently differentiated across the four genes that 100bp

139 reads align unambiguously to one location in the genome.[37] Reads were detected in 5N and 5A

140 for all samples, across all four genes, with the exception of the *SCN1A* for which 31 of 176

141 samples (17.6%) had no detectable 5N reads (Fig. 2A). Along with quantifying the expression of

142 5N and 5A (Fig. 2), we also assessed expression for the surrounding constitutive exons, as a

143 control (Fig. S2). For the mouse cortical data, the same analysis methods were used but with

144 alternative references, specifically the GRCm38/mm10 genome and GENCODE vM25 gene

145 definitions. A similar approach was used to assess the utilization of 18N and 18A in *SCN8A*.

146

147 **2.3 Intron splicing**

148 We applied a complementary approach to detecting 5N and 5A exon usage by assessing intron

149 splicing via reads that map across exon-exon junctions in the same 176 BrainVar samples. Reads

150 were aligned with OLego aligner[38] using the same genome build and gene definitions as for

151 exon expression. Clusters of differential intron splicing were identified with Leafcutter[39] and

152 differences across development were detected by comparing 112 prenatal samples to 60

153 postnatal samples. No cluster was detected for 5N/5A in *SCN1A*, preventing assessment across

154 development, but clusters were identified and assessed for the other three genes and for

155 18N/18A in *SCN8A* (Figs. 3, 5).

156

157 **2.4 Quantitative trait locus (QTL) analysis**

158 Common variants with a minor allele frequency ≥5% in both the prenatal (N = 112) and

159 postnatal (N = 60) samples and Hardy Weinberg equilibrium p value ≥ $1x10^{-12}$ were identified

160 previously.[32] Variants within one million basepairs of each sodium channel gene were extracted

161 and integrated with the Leafcutter clusters, along with the first five principal components

162 calculated from common variants identified in whole-genome sequencing data from these

163 samples and 3,804 parents from the Simons Simplex Collection[32,40] to predict sQTLs with

164 FastQTL.[41] This analysis was performed on all samples, prenatal-only samples, and postnatal-

165   only samples, with false discovery rate (FDR) estimated from the results of each analysis using
166   the Benjamini-Hochberg procedure.[42] To assess correlation of 5N expression for the SNP
167   rs3812718, genotypes were extracted for chr2:166,053,034 C>T (GRCh38) and compared with
168   5N expression calculated by DEXSeq, as described above.
169
170   **2.5 Statistical analysis**
171   The 5N:5A expression ratio was calculated from normalized exon expression values (CPM).
172   Linear regression was used to assess whether this ratio varied across development by
173   comparing the log-transformed 5N:5A ratio to log-transformed post-conceptual days (Fig. 2).
174   The difference in ratio was also assessed between the mid-late fetal samples (N=112) and
175   childhood/adolescent/young adult samples (N=35) with a two-tailed Wilcoxon test. To compare
176   intron splicing between prenatal and postnatal samples, we used the P-values estimated with a
177   Dirichlet-multinomial generalized linear model, as implemented in Leafcutter.[39]
178
179   **3. Results**
180
181   **3.1 Expression of voltage-gated sodium channels in the human cortex**
182   Gene expression varies dramatically across development for many genes, especially during the
183   late-fetal transition, during which half the genes expressed in the brains undergo a concerted
184   increase or decrease in expression.[12,32,43,44] To assess gene-level developmental trajectories, we
185   analyzed bulk-tissue RNA-seq of the human DLPFC in 176 *post mortem* samples from the
186   BrainVar cohort (104 male, 72 female, spanning 6 post-conceptual weeks to 20 years after
187   birth).[32] The gene-level expression profile of all four voltage-gated sodium channels changes
188   during this late-fetal transition (Fig. 1F-I), with *SCN1A*, *SCN2A*, and *SCN8A* expression rising from
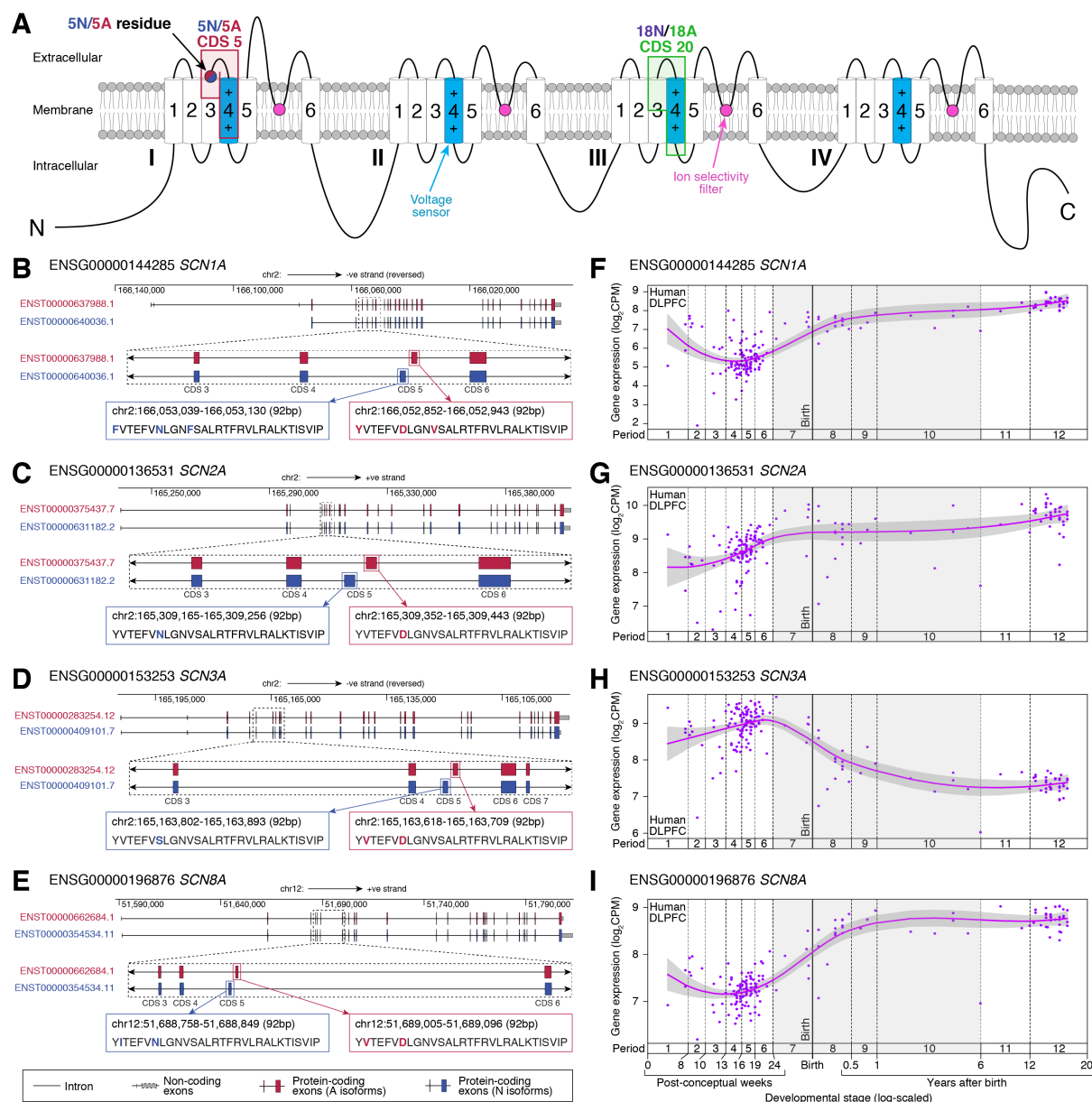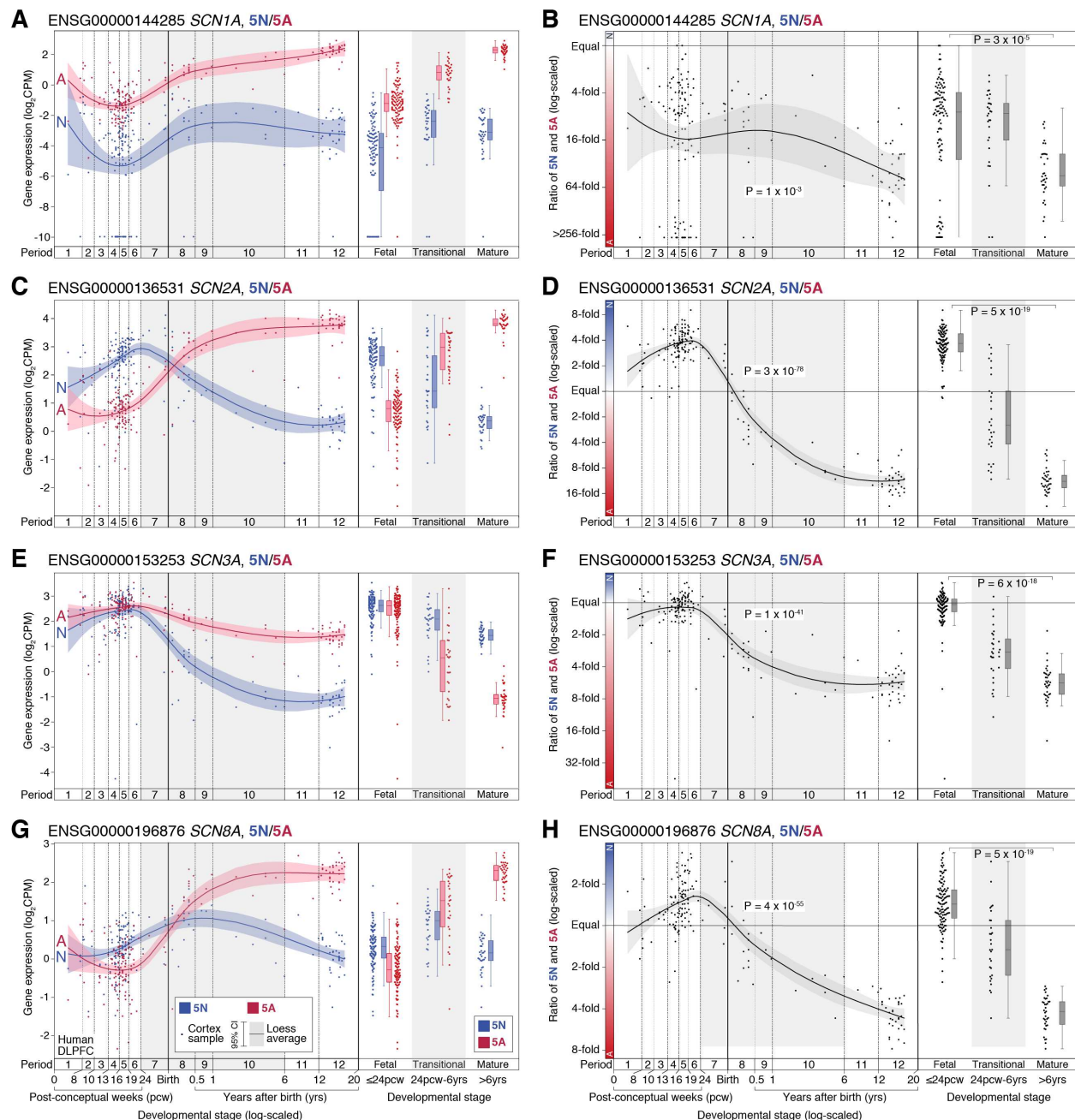189   mid-fetal development through infancy to early childhood, while *SCN3A* expression falls.
190

Figure 1. Splicing isoforms in voltage-gated sodium channels. A) Voltage-gated sodium channels are composed of four similar domains (I, II, III, IV), each of which includes six transmembrane segments with extracellular or intracellular linkers. The fourth transmembrane segment (S4) in each domain acts as a voltage sensor. Between the fifth and sixth transmembrane segment (S5, S6) is a pore loop that forms the ion selectivity filter. The fifth protein-coding exon (5N/5A, CDS 5) encodes a portion of the first domain, while the 20th protein-coding exon (18N/18A, CDS 20) encodes a similar portion of the third domain. **B)** Location, genomic coordinates (GRCh38/hg38), and amino acid sequence of the '5A' and '5N' exons four sodium channels. **C)** Patterns of whole-gene expression in the human dorsolateral prefrontal cortex (DLPFC) across prenatal and postnatal development from the BrainVar dataset [32]. CPM: counts per million. Genomic coordinates are based on GRCh38/hg38 using GENCODE v31 gene definitions.

3.2 Developmental trajectories of 5N and 5A expression in the human cortex

The majority of protein-coding exons follow the expression trajectory of their parent gene across development (Fig. S3), however all four sodium channels show dynamic changes in the utilization of 5N/5A (Fig. 2). This is especially marked for *SCN2A* and *SCN8A*, where 5N is
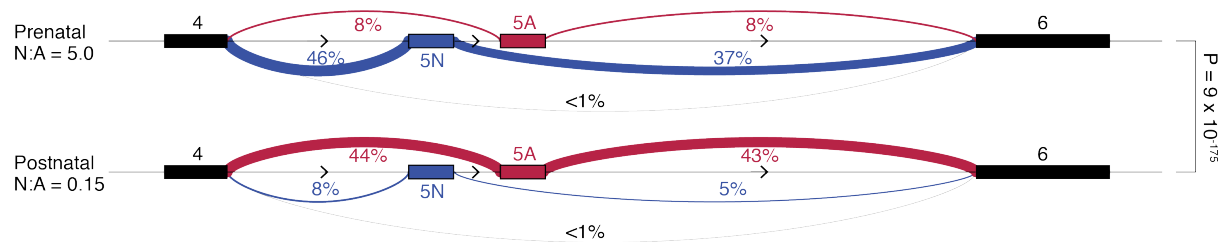
207   expressed at a higher level than 5A in the mid-fetal brain but this reverses soon after birth.
208   Plotting the 5N:5A ratio allows exon utilization to be assessed independent of changes in gene
209   expression (Fig. 2). All four genes show changes in the N:A ratio across development, with a
210   modest change for *SCN1A* (0.14 fetal to 0.02 childhood/adolescent; p=0.00003, two-sided
211   Wilcoxon test, Figure 2B) and dramatic changes for *SCN2A* (3.7 to 0.09; p=5×10^{-19}, Fig. 2D),
212   *SCN3A* (0.96 to 0.18; p=6×10^{-18}, Fig. 2F), and *SCN8A* (3.7 to 0.09; p=5×10^{-19}, Fig. 2H). As a
213   control, we applied this approach to assess the ratio of CDS 4 and CDS 6 across development.
214   We observed no developmental shift in the 4:6 ratio for *SCN1A*, *SCN2A*, and *SCN3A*, however
215   the exon 4:6 ratio is marginally higher than expected in the prenatal period for *SCN8A* (0.82 vs.
216   0.66; 9×10^{-10}, Fig. S2). This developmental variation in *SCN8A* is not observed for the
217   surrounding protein-coding exons and reflects a modest increase in CDS 4 expression in the
218   prenatal period, based on the expected expression given the exon length (Fig. S4).
219

Figure 2. Expression of 5N and 5A in the human cortex across development. A) The expression of 5N (blue) and 5A (red) in *SCN1A* is shown for 176 BrainVar human cortex (DLPFC) samples across development (points). On the left, the colored line shows the Loess smoothed average and 95% confidence interval (shaded region). On the right, boxplots show the median and interquartile range for the same data, binned into fetal, transitional, and mature developmental stages. **B)** The ratio of 5N and 5A expression from panel 'A' is shown across development (left) and in three developmental stages (right). **C-H)** Panels A and B are repeated for the genes *SCN2A*, *SCN3A*, *SCN8A*. For comparison, the same plots for CDS four and six are shown in Figure S2. CPM: Counts per million; DLPFC: Dorsolateral prefrontal cortex. Statistical tests: B, D, F, H) Left panel, linear regression of $\log_2$(5N:5A ratio) and $\log_2$(post-conceptual days). Right panel, two-tailed Wilcoxon test of $\log_2$(5N:5A ratio) values between fetal and mature groups.
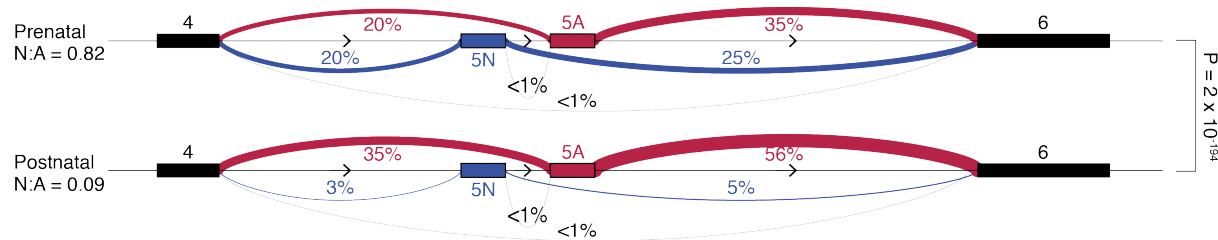
3.3 Intron splicing around 5N and 5A in the human cortex

233   To verify that mutually exclusive use of 5N and 5A underlies the observed exon expression
234   changes (Fig. 2), we considered RNA-seq reads that spanned exon-exon junctions to quantify
235   intron splicing. Clusters of differential intron splicing corresponding to 5N/5A usage were
236   identified by Leafcutter for *SCN2A*, *SCN3A*, and *SCN8A* (Fig. 3), but not *SCN1A*, likely due to the
237   consistently low expression of N isoforms (Fig. 2). The splicing patterns for *SCN2A*, *SCN3A*, and
238   *SCN8A* are consistent with the observed exon expression changes (Fig. 2, 3) and at least 99% of
239   reads are consistent with mutually exclusive 5N/A utilization.
240

A ENSG00000136531 *SCN2A*

B ENSG00000153253 *SCN3A* (reversed)

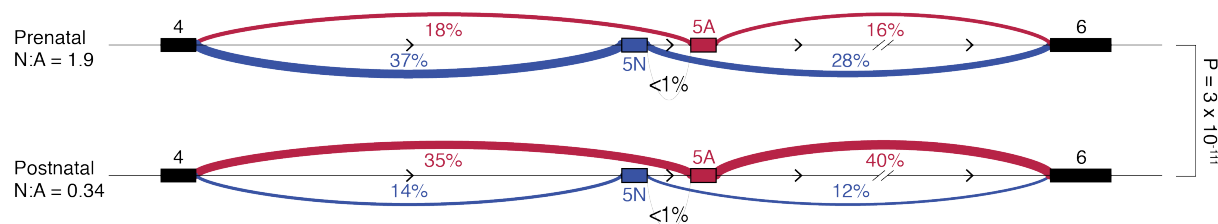**C** ENSG00000196876 *SCN8A*

241
242
243   **Figure 3. Intron splicing of sodium channel genes in the developing human cortex. A)** Sashimi plot of splicing in the prenatal
244   (top, N=112 samples) and postnatal (bottom, N=60 samples) DLPFC for *SCN2A*. Linewidth is proportional to percentage of split
245   reads observed for each intron and this value is given as a percentage. Introns related to 5N inclusion are shown in blue, those
246   related to 5A inclusion are shown in red, and others are in grey. **B-C)** Equivalent plots for *SCN3A* (a negative strand gene with
247   the orientation reversed to facilitate comparison to the other two genes) and *SCN8A*. P-values compare the prenatal and
248   postnatal cluster using a Dirichlet-multinomial generalized linear model, as implemented in Leafcutter.[39]
249

250   **3.4 Developmental trajectories of 5N and 5A expression in the mouse cortex**
251   We repeated the analysis of sodium channel 5N/5A expression using bulk tissue RNA-seq data
252   from the mouse cortex across development (N=58; E15.5 to P75). Our data are consistent with
253   the N:A ratios described previously.[20] We observe more substantial differences at the extremes
254   of development: *SCN2A* (3.3 fetal to 0.06 mature; p=0.00003, two-sided Wilcoxon test, Fig. 4C),

255 *SCN3A* (2.4 to 0.14; p=0.00008, Fig. 4E), and *SCN8A* (1.8 to 0.22; p=0.00003, Fig. 4G). Mice lack a
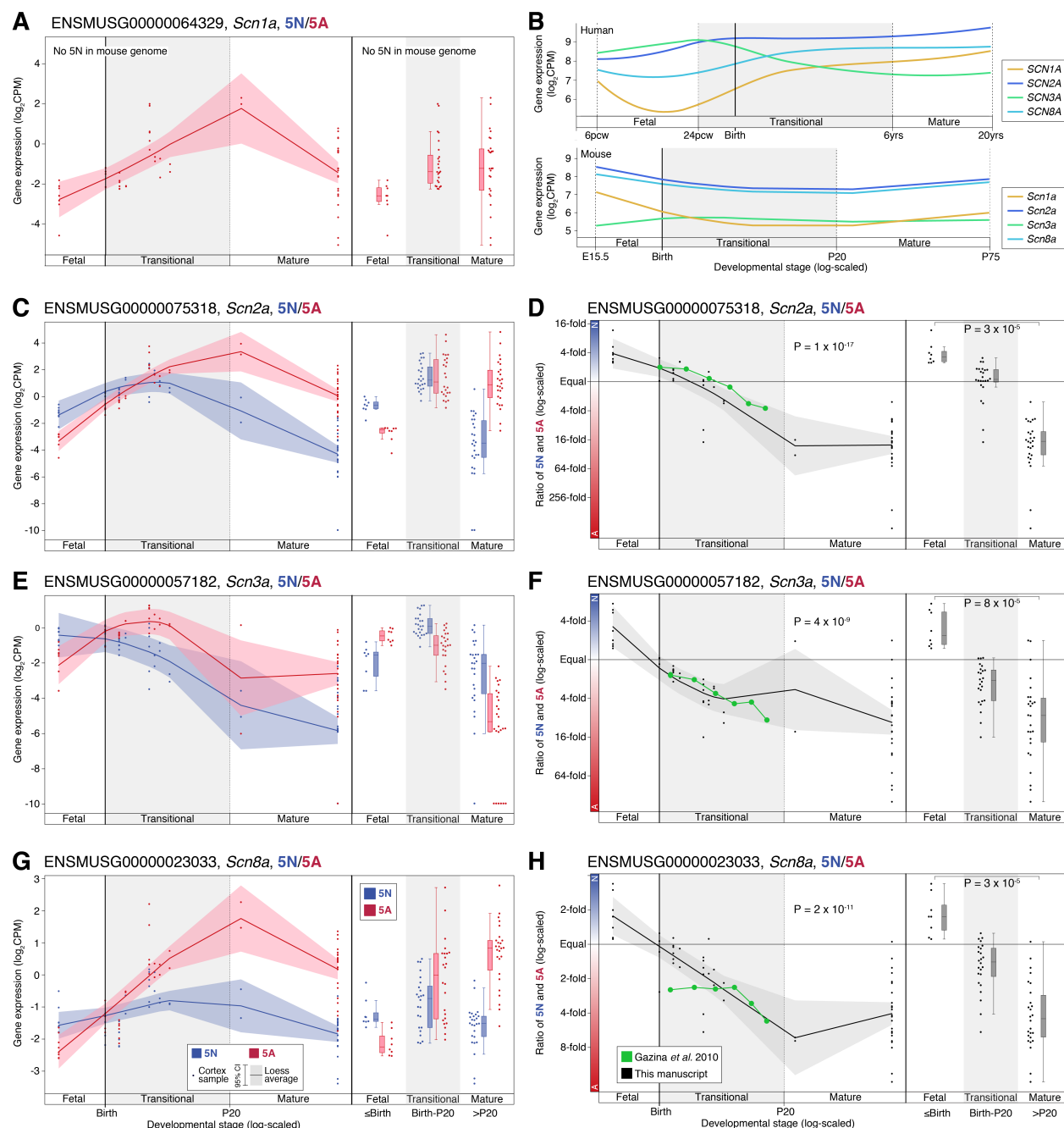256 functional 5N exon in *SCN1A*.

257

258
259 **Figure 4. Expression of 5N and 5A in the mouse cortex across development. A)** The expression of 5A (red) in *Scn1a* is shown
260 for 58 mouse cortex samples across development (points); no functional 5N equivalent is present in the mouse genome. On the
261 left, the colored line shows the Loess smoothed average and 95% confidence interval (shaded region). On the right, boxplots
262 show the median and interquartile range for the same data, binned into fetal, transitional, and mature developmental stages.
263 **B)** The Loess smoothed average expression of the four voltage-gated sodium channels in human cortex (top, Fig. 1) and mouse
264 cortex (bottom). **C)** Panel 'A' is repeated for *Scn2a* with the inclusion of 5N (blue). **D)** The ratio of 5N and 5A expression from
265 panel 'C' is shown across development (left) and in three developmental stages (right). Values reported previously in mouse
266 cortex are shown in the same scale in green for comparison [20]. **E-H)** Panels 'C' and 'D' are repeated for the genes *Scn3a*, *Scn8a*.

267 CPM: Counts per million. Statistical tests: D, F, H) Left panel, linear regression of $\log_2$(5N:5A ratio) and $\log_2$(post-conceptual
268 days). Right panel, two-tailed Wilcoxon test of $\log_2$(5N:5A ratio) values between fetal and mature groups.
269

270 **3.5 No evidence of common polymorphisms regulating 5N or 5A utilization**
271 A common polymorphism (rs3812718, GRCh38 chr2:166,053,034 C>T, IVS5N+5G>A) has
272 previously been associated with epilepsy, seizures, and response to anti-epileptics,[21,22,26,45,46]
273 though this variant did not reach genome-wide significance in a mega-analysis of epilepsy.[47]
274 Prior analyses of expression in the adult human temporal cortex showed evidence that the
275 homozygous variant allele (TT in DNA, AA in cDNA) was associated with reduced utilization of
276 5N.[21,48] We do not observe evidence for such a relationship in the prenatal or postnatal
277 prefrontal cortex (Fig. S5) and this polymorphism is not identified as a splicing quantitative trait
278 locus (QTL) in GTEx.[49] Furthermore, this variant is not predicted to alter splicing behavior using
279 the SpliceAI algorithm.[50] The TT genotype is associated with increased expression of *SCN1A* in
280 the adult human basal ganglia with (p=1x10^{-10}).[49]
281

282 **3.6 Developmental trajectories of 18N and 18A expression in *SCN8A***
283 We next considered the developmental timing of the transition between 18N and 18A in *SCN8A*
284 (Fig. 1A, 5A). Intron splicing shows a robust difference between prenatal and postnatal human
285 dorsolateral prefrontal cortex (P = 4 x 10^{-185}, Fig. 5B), with the prenatal period characterized by
286 high frequencies of transcripts excluding 18A, either including 18N or skipping both 18N and
287 18A, while in the postnatal cortex 18A is included in 93% of reads. Considering exon expression
288 (Fig. 5C, 5D), the expression of 18A increases markedly over development and this is distinct
289 from other protein-coding exons for *SCN8A* (Fig. S3). The 18N/18A transition begins around 13
290 post-conceptual weeks and continues till six months-of-age, with both timepoints being earlier
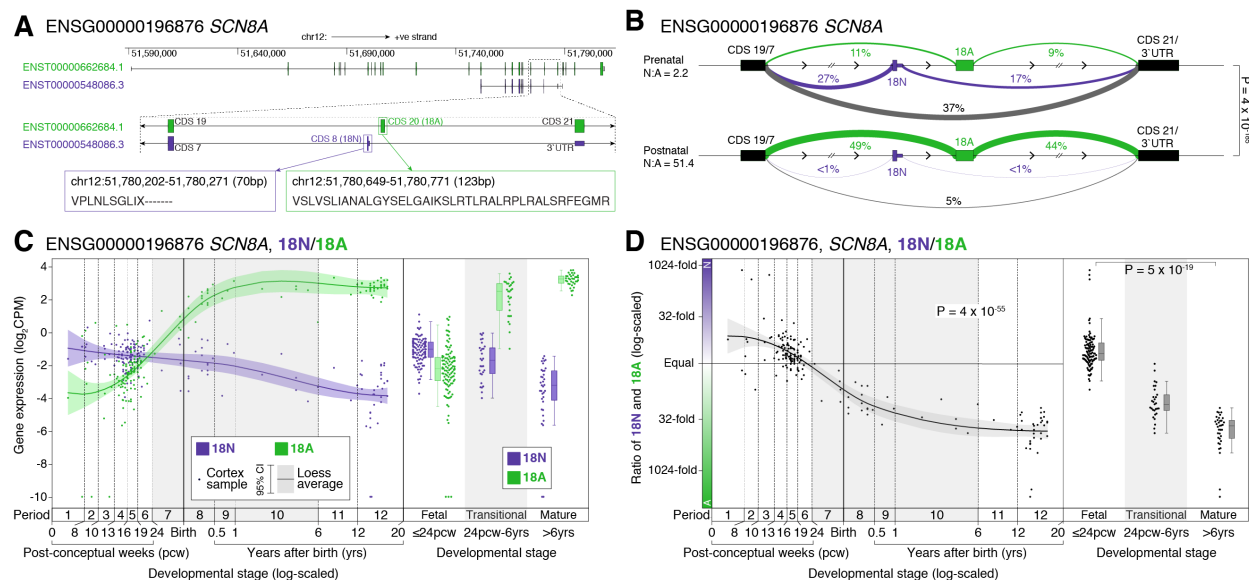291 than the equivalents for 5N/5A in *SCN8A* and the other genes.
292

293
294 **Figure 5. Developmental trajectories of CDS 20 (18N/18A) in human cortex in *SCN8A*. A)** Location, genomic coordinates
295 (GRCh38/hg38), and amino acid sequence of the 18N and 18A exons in *SCN8A*. **B)** Sashimi plot of intron splicing in the prenatal
296 (top, N=112 samples) and postnatal (bottom, N=60 samples) dorsolateral prefrontal cortex. Linewidth is proportional to
297 percentage of reads observed for each exon-exon junction and this value is also shown as a percentage. Introns related to 18N
298 exon inclusion are shown in purple, those related to 18A exon inclusion are shown in green, and others are in grey. **C)**

299 Expression of the 18N (purple) and 18A (green) for 176 BrainVar human dorsolateral prefrontal cortex samples across
300 development (points). On the left, the colored line shows the Loess smoothed average with the shaded area showing the 95%
301 confidence interval. On the right, boxplots show the median and interquartile range for the same data, binned into fetal,
302 transitional, and mature developmental stages. **D)** The 18N:18A ratio is shown for each sample from panel 'C' across
303 development (left) and binned into three groups (right). CPM: Counts per million; Statistical analyses: B) Dirichlet-multinomial
304 generalized linear model, as implemented in Leafcutter,[39] D) Left panel, linear regression of $\log_2$(18N:18A ratio) and $\log_2$(post-
305 conceptual days). Right panel, two-tailed Wilcoxon test of $\log_2$(18N:18A ratio) values between fetal and mature groups.
306

307 **3.7 Other annotated protein-coding exons with distinct developmental trajectories**
308 To assess whether other protein-coding exons undergo distinct developmental transitions (Fig.
309 S3), we calculated the ratios of all pairs of protein-coding exons within each for the four sodium
310 channel genes and assessed whether the ratio was correlated with development stage using
311 linear regression. This is the same calculation used to quantify the 5N/5A and 18N/18A
312 transitions (Fig. 2, 5D) and distinguishes exons with expression profiles that differ from the rest
313 of the gene (e.g. 5A in *SCN2A*), rather than simply being expressed at reduced levels, suggesting
314 alternative regulatory processes (Fig. S3). Visualizing the R^2 values of these correlations
315 provides simple method to identify the such distinct trajectories (Fig. 6). Aside from 5N/5A and,
316 in *SCN8A*, 18N/18A, no protein-coding exons common to most isoforms (consistent CDS in Fig.
317 S3) show differential expression, but a few weakly expressed protein-coding exons specific to a
318 small number of isoforms (variable CDS in Fig. S3) do vary across development (Fig. 6).
319

320 GENCODE defines seven variable CDS exons for *SCN1A* (DEXSeq divisions: 006, 015, 021, 031,
321 034, 047, 049; Table S2, Fig. 6A). Of these, only 021 shows a distinct developmental trajectory
322 (Fig. 6A), with reduced postnatal expression relative to other *SCN1A* exons (Fig. S3). This result
323 is verified by the intron splicing data (p = 6 x 10^{-91}, Leafcutter).
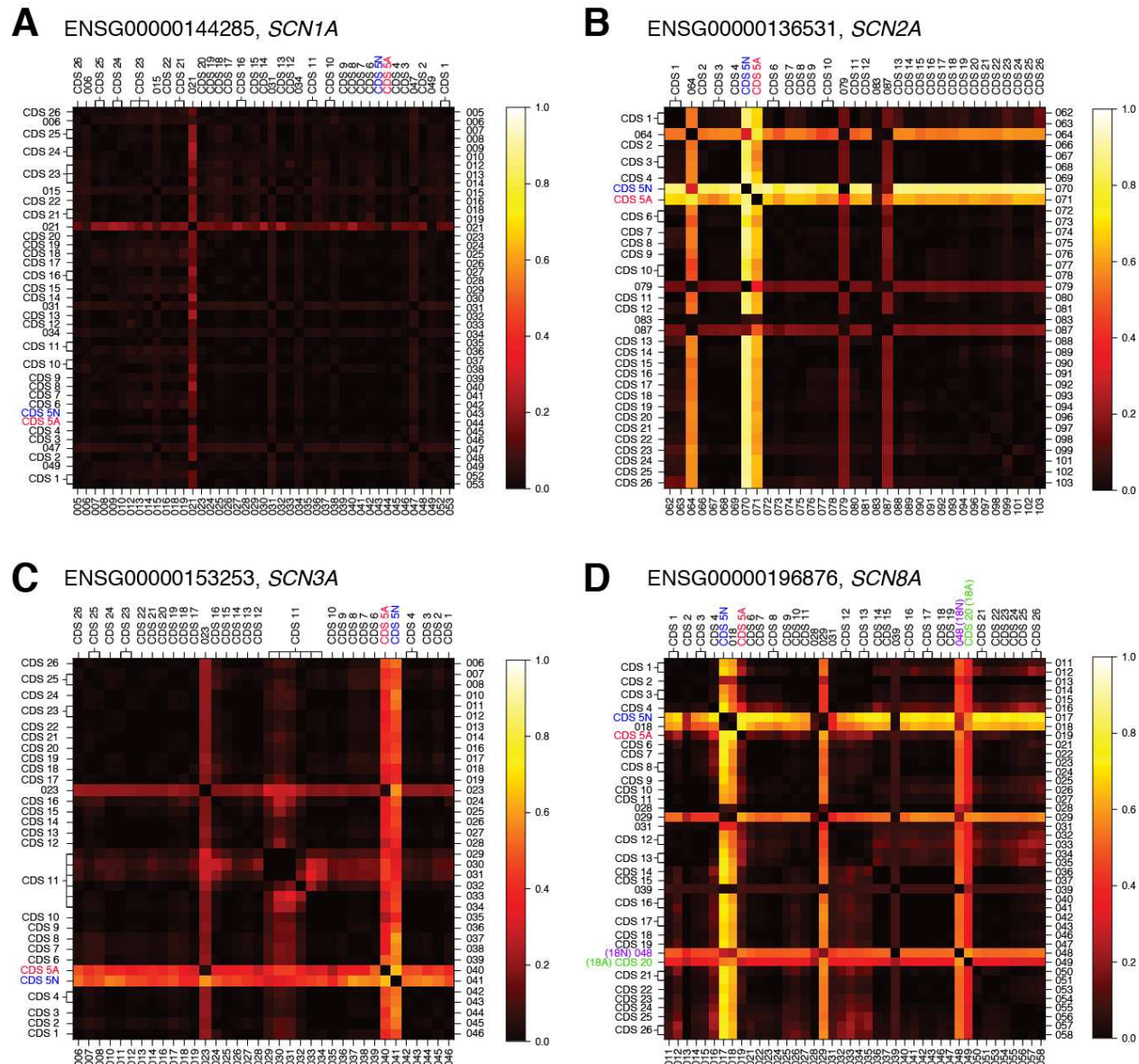324

Figure 6. Identification of protein-coding exons with complex developmental trajectories. A) The correlation between the ratio of CPM expression between pairs of exons (log-scaled) and developmental stage (post conceptual days, log-scaled) for *SCN1A* was assessed with a linear model (e.g. Fig. 2B). The R^2 value of each exon pair is show as a heat map with 'hot' colors representing exon-pairs with high R^2 values for which variation in the ratio is correlated with developmental age, i.e. pairs of exons that show substantially different expression across development. Exon numbers from DEXSeq (Table S2) are shown on the bottom and right and equivalent CDS number on the top and left (see Table S2). **B-D)** The analysis is repeated for *SCN2A*, *SCN3A*, and *SCN8A*.

In *SCN2A*, the 5N/5A trajectories stand out clearly (Fig. 6B). There are four variable CDS exons (DEXSeq divisions: 064, 079, 083, 087; Table S2, Fig. 6B), three of which have distinct developmental trajectories (Fig. 6B, S3): 064 (Fig. S3, P = 2 x 10^{-12}, Leafcutter), 079 (Fig. S3, P = 7 x 10^{-33}, Leafcutter), 087 (Fig. S3, P = 2 x 10^{-20}, Leafcutter). The single variable CDS exon in *SCN3A*, 023 (Table S2, Fig. 6C), varies across development (Fig. S3, P = 3 x 10^{-80}, Leafcutter). Finally, aside from 18N, there are five variable CDS exons in *SCN8A* (DEXSeq divisions: 018, 028,

341   029, 031, 039; Table S2, Fig. 6D) of which 018 and 029 vary across development (Fig. 6D), but
342   neither of these are validated by Leafcutter.

Discussion

345   Using transcriptomic data from 176 human dorsolateral prefrontal cortex samples, we
346   characterized the developmental patterns for all protein-coding exons in *SCN1A*, *SCN2A*,
347   *SCN3A*, and *SCN8A* (Fig. 6, S3). We observed a coordinated decrease in the 5N:5A ratio between
348   24 post-conceptual weeks (2nd trimester) and six years-of-age that is synchronized with
349   widespread transcriptomic changes in the brain during the late-fetal transition.[32,44] This is
350   preceded by a similar decrease in the 18N:18A ratio in *SCN8A* from 13 post-conceptual weeks
351   to 6 months-of-age, which is regulated by *RBFOX1*. By analyzing a wider developmental window
352   than prior analyses[20,21,48] we observed more dynamic changes and larger disparities in exon
353   expression.

355   Recent advances have shown that differential splicing patterns can be effective therapeutic
356   targets in humans, for example through intrathecal antisense oligonucleotides.[51,52] Since the
357   electrophysiological consequences of some epileptic encephalopathy associated variants differ
358   between 5N and 5A, manipulating this ratio may offer therapeutic benefit in individuals
359   carrying these variants. We consider three therapeutic scenarios.

361   First, for individuals with disorder-associated genetic variants within the 30 amino acids
362   encoded by the 5th exon, expressing the other copy of the 5th exon could skip the variant.
363   Theoretically, this approach could benefit individuals with both loss-of-function (protein-
364   truncating variants, missense, splice site) and gain-of-function (missense) variants in the 5th
365   exon. At present, ten such cases have been identified, all with epileptic encephalopathy
366   variants identified in the 5A exon of *SCN2A* and *SCN8A*.[53,54] Since the total transcript level
367   would be unchanged, this strategy may provide a wider therapeutic window than simply
368   decreasing expression levels. The success of the therapy would depend upon the proportion of
369   transcripts expressing the alternate 5th exon and the ability of this exon to functionally replace
370   the original 5th exon.

372   Second, splice isoforms can also have an effect on the biophysical effects of variants outside the
373   5th exon. For example, three recently characterized epileptic encephalopathy associated
374   variants in *SCN2A*—T236S, E999K, and S1336Y—all exhibit more pronounced alterations in their
375   electrophysiological properties in 5N $Na_v1.2$ isoforms.[23] Two other epileptic encephalopathy-
376   associated variants—M252V and L1563V—exhibit biophysical changes only when expressed on
377   5N isoform.[14,55] For individuals with these mutations, tilting expression towards the 5A isoform
378   could provide some symptomatic improvement, especially during infancy. Including both the
379   5N and 5A isoforms in functional characterization of variant impact may identify many more
380   such variants.[23]

382   Finally, modifying splicing might aid seizure control in older children and adults. At this age, the
383   5A isoform is predominantly utilized in both *SCN2A* or *SCN8A*, which are mainly expressed in

384   glutamatergic neurons.[11] Reverting expression to the fetal/neonatal state by encouraging 5N
385   utilization could reduce the excitability of cortical glutamatergic neurons, potentially
386   limiting seizures. Since this would require repeated intrathecal administration, it would likely be
387   limited to the most severe cases of epilepsy. Furthermore, it remains to be seen whether this
388   approach could offer therapeutic benefits above and beyond existing antiepileptic drugs.
389
390   Our analysis was limited by the use of short-read transcriptomic data, leading us to focus on
391   quantifying exon-level expression (Fig. 2) and splice junction usage (Fig. 3), rather than relying
392   on estimates of isoform utilization (Fig. S1). We also elected to focus on protein-coding
393   transcripts and exons defined by GENCODE (v31) rather than attempting *de novo* transcriptome
394   assembly. Emerging long-read transcriptomic technology may substantially expand estimates of
395   isoform and exon diversity but these technologies have not been applied to the developing
396   human brain at scale.[56,57] We also note that transcriptomic data is only partially predictive of
397   protein levels and other factors, including channel transport and degradation, may influence
398   the impact of isoforms on neuronal function. Comparing the human and mouse cortex data
399   (Figs. 2, 4), it is possible that more substantial differences in gene and exon expression may be
400   observed at earlier embryonic times in the mouse or with larger sample sizes. In addition, the
401   use of bulk-tissue transcriptomic data limits our ability to assess how individual cell-types or
402   cell-states contribute to the observed isoform trajectories. Technological and methodological
403   advances may provide insights at cell-level resolution in the future.[58]
404
405   **Conclusion**
406   Dramatic differences in exon usage of *SCN1A*, *SCN2A*, *SCN3A*, and *SCN8A* observed in rodent
407   brains also occur in the human developing cortex, beginning in mid-fetal development and
408   continuing through childhood. These changes in splicing affect the biophysical properties of the
409   encoded channels and are likely to contribute to differences in phenotype observed between
410   individuals with different variants and across development.
411

421   **Author Contributions**
422   Experimental design, S.J.S.; Data generation, L.L., S.F.D., S.P., F.O.G., A.S., J.Y.A., and J.L.R.R.;
423   Data processing, L.L., M.C.G., B.K.S., and D.M.W.; Data analysis, L.L., D.M.W., and S.J.S.;
424   Statistical analysis, S.J.S.; Manuscript preparation, L.L., K.J.B., and S.J.S.
425

426   **Declaration of interests**

427   J.L.R.R. is cofounder, stockholder, and currently on the scientific board of *Neurona*, a company

428   studying the potential therapeutic use of interneuron transplantation.

References

1. Heyne HO, Singh T, Stamberger H, Abou Jamra R, Caglayan H, Craiu D, et al. De novo variants in neurodevelopmental disorders with epilepsy. Nat Genet [Internet]. 2018; :1. Available from: http://www.nature.com/articles/s41588-018-0143-7

2. Satterstrom FK, Kosmicki JA, Wang J, Breen MS, De Rubeis S, An J-Y, et al. Large-Scale Exome Sequencing Study Implicates Both Developmental and Functional Changes in the Neurobiology of Autism. Cell. 2020; .

3. Kaplanis J, Samocha KE, Wiel L, Zhang Z, Arvai KJ, Eberhardt RY, et al. Integrating healthcare and research genetic data empowers the discovery of 49 novel developmental disorders. bioRxiv [Internet]. 2019; :797787. Available from: http://biorxiv.org/content/early/2019/10/16/797787.abstract

4. Catterall WAWA, Marban E, Catterall WAWA, Cestèle S, Catterall WAWA, Wood JN, et al. Voltage-gated sodium channels. J Physiol [Internet]. 2001; 1(1):17–21. Available from: http://www.pubmedcentral.nih.gov/articlerender.fcgi?artid=3885250&tool=pmcentrez&rendertype=abstract%5Cnhttp://www.pubmedcentral.nih.gov/articlerender.fcgi?artid=3424717&tool=pmcentrez&rendertype=abstract%5Cnhttp://onlinelibrary.wiley.com/doi/10.1111/j.14

5. Bender KJ, Trussell LO. The physiology of the axon initial segment. Annu Rev Neurosci. 2012; 35(1):249–65.

6. Kole MHP, Stuart GJ. Signal processing in the axon initial segment. Neuron [Internet]. 2012; 73(2):235–47. Available from: http://dx.doi.org/10.1016/j.neuron.2012.01.007

7. Spratt PWE, Ben-Shalom R, Keeshen CM, Burke KJJ, Clarkson RL, Sanders SJ, et al. The Autism-Associated Gene Scn2a Contributes to Dendritic Excitability and Synaptic Function in the Prefrontal Cortex. Neuron. 2019; 103(4):673-685.e5.

8. Hu W, Tian C, Li T, Yang M, Hou H, Shu Y. Distinct contributions of Na(v)1.6 and Na(v)1.2 in action potential initiation and backpropagation. Nat Neurosci [Internet]. 2009; 12(8):996–1002. Available from: http://www.ncbi.nlm.nih.gov/pubmed/19633666

9. Smith RS, Kenny CJ, Ganesh V, Jang A, Borges-Monroy R, Partlow JN, et al. Sodium Channel SCN3A (Na(V)1.3) Regulation of Human Cerebral Cortical Folding and Oral Motor Development. Neuron. 2018; 99(5):905-913.e7.

10. Berret E, Barron T, Xu J, Debner E, Kim EJ, Kim JH. Oligodendroglial excitability mediated by glutamatergic inputs and Nav1.2 activation. Nat Commun [Internet]. 2017; 8(1). Available from: http://dx.doi.org/10.1038/s41467-017-00688-0

11. Brunklaus A, Du J, Steckler F, Ghanty II, Johannesen KM, Fenger CD, et al. Biological concepts in human sodium channel epilepsies and their relevance in clinical practice. Epilepsia. 2020; 61(3):387–99.

12. Kang HJ, Kawasawa YI, Cheng F, Zhu Y, Xu X, Li M, et al. Spatio-temporal transcriptome of the human brain. Nature [Internet]. 2011; 478(7370):483–9. Available from: http://www.ncbi.nlm.nih.gov/pubmed/22031440

13. Wolff M, Johannesen KM, Hedrich UBS, Masnada S, Rubboli G, Gardella E, et al. Genetic and phenotypic heterogeneity suggest therapeutic implications in SCN2A-related disorders. Brain [Internet]. 2017; . Available from: https://academic.oup.com/brain/article-lookup/doi/10.1093/brain/awx054

14. Liao Y, Anttonen A-K, Liukkonen E, Gaily E, Maljevic S, Schubert S, et al. SCN2A mutation associated with neonatal epilepsy, late-onset episodic ataxia, myoclonus, and pain. Neurology. 2010; 75(16):1454–8.

15. Tian C, Wang K, Ke W, Guo H, Shu Y. Molecular identity of axonal sodium channels in human cortical pyramidal cells. Front Cell Neurosci [Internet]. 2014; 8(September):297. Available from: http://journal.frontiersin.org/article/10.3389/fncel.2014.00297/abstract

16. Plummer NW, McBurney MW, Meisler MH. Alternative splicing of the sodium channel SCN8A predicts a truncated two-domain protein in fetal brain and non-neuronal cells. J Biol Chem. 1997; 272(38):24008–15.

17. Gustafson TA, Clevinger EC, Neill TJO, Yarowskys PJ, Kruegerg BK. Mutually exclusive exon splicing of type III brain sodium channel alpha subunit RNA generates developmentally regulated isoforms in rat brain. J Biol Chem. 1993; 268(25):18648–53.

18. Zaman T, Helbig KL, Clatot J, Thompson CH, Kang SK, Stouffs K, et al. SCN3A-Related Neurodevelopmental Disorder: A Spectrum of Epilepsy and Brain Malformation. Ann Neurol. 2020; .

19. Zaman T, Helbig I, Božović IB, DeBrosse SD, Bergqvist AC, Wallis K, et al. Mutations in SCN3A cause early infantile epileptic encephalopathy. Ann Neurol. 2018; 83(4):703–17.

20. Gazina E V, Richards KL, Mokhtar MBC, Thomas E a, Reid C a, Petrou S. Differential expression of exon 5 splice variants of sodium channel alpha subunit mRNAs in the developing mouse brain. Neuroscience [Internet]. 2010; 166(1):195–200. Available from: http://www.ncbi.nlm.nih.gov/pubmed/20006674

21. Tate SK, Depondt C, Sisodiya SM, Cavalleri GL, Schorge S, Soranzo N, et al. Genetic predictors of the maximum doses patients receive during clinical use of the anti-epileptic drugs carbamazepine and phenytoin. Proc Natl Acad Sci U S A. 2005; 102(15):5507–12.

22. Tate SK, Singh R, Hung CC, Tai JJ, Depondt C, Cavalleri GL, et al. A common polymorphism in the SCN1A gene associates with phenytoin serum levels at maintenance dose. Pharmacogenet Genomics. 2006; 16(10):721–6.

23. Thompson CH, Ben-Shalom R, Bender KJ, George AL. Alternative splicing potentiates dysfunction of early-onset epileptic encephalopathy SCN2A variants. J Gen Physiol. 2020; 152(3):1–16.

24. Kasai N, Fukushima K, Ueki Y, Prasad S, Nosakowski J, Sugata KI, et al. Genomic structures of SCN2A and SCN3A - Candidate genes for deafness at the DFNA16 locus. Gene. 2001; 264(1):113–22.

25. Copley RR. Evolutionary convergence of alternative splicing in ion channels. Trends Genet. 2004; 20(4):171–6.

507   26.   Thompson CH, Kahlig KM, George AL. SCN1A splice variants exhibit divergent sensitivity
508   to commonly used antiepileptic drugs. Epilepsia. 2011; 52(5):1000–9.

509   27.   Diss JKJ, Fraser SP, Djamgoz MBA. Voltage-gated Na+ channels: Multiplicity of expression,
510   plasticity, functional implications and pathophysiological aspects. Eur Biophys J. 2004;
511   33(3):180–93.

512   28.   Gazina E V., Leaw BTWW, Richards KL, Wimmer VC, Kim TH, Aumann TD, et al.
513   "Neonatal" Nav1.2 reduces neuronal excitability and affects seizure susceptibility and
514   behaviour. Hum Mol Genet. 2015; 24(5):1457–68.

515   29.   O'Brien JE, Drews VL, Jones JM, Dugas JC, Barres BA, Meisler MH. Rbfox proteins regulate
516   alternative splicing of neuronal sodium channel SCN8A. Mol Cell Neurosci [Internet].
517   2012; 49(2):120–6. Available from: http://dx.doi.org/10.1016/j.mcn.2011.10.005

518   30.   Zubović L, Baralle M, Baralle FE. Mutually exclusive splicing regulates the Nav 1.6 sodium
519   channel function through a combinatorial mechanism that involves three distinct splicing
520   regulatory elements and their ligands. Nucleic Acids Res. 2012; 40(13):6255–69.

521   31.   Harrow J, Frankish A, Gonzalez JM, Tapanari E, Diekhans M, Kokocinski F, et al.
522   GENCODE: the reference human genome annotation for The ENCODE Project. Genome
523   Res [Internet]. 2012; 22(9):1760–74. Available from:
524   http://www.ncbi.nlm.nih.gov/pubmed/22955987

525   32.   Werling DM, Pochareddy S, Choi J, An J-YY, Sheppard B, Peng M, et al. Whole-Genome
526   and RNA Sequencing Reveal Variation and Transcriptomic Coordination in the Developing
527   Human Prefrontal Cortex. Cell Rep. 2020; 31(1):107489.

528   33.   MacLaren R, Radcliffe RA, Van Matre ET, Robertson CE, Ir D, Frank DN. The Acute
529   Influence of Acid Suppression with Esomeprazole on Gastrointestinal Microbiota and
530   Brain Gene Expression Profiles in a Murine Model of Restraint Stress. Neuroscience
531   [Internet]. 2019; 398:206–17. Available from:
532   https://doi.org/10.1016/j.neuroscience.2018.11.048

533   34.   Dobin A, Davis CA, Schlesinger F, Drenkow J, Zaleski C, Jha S, et al. STAR: ultrafast
534   universal RNA-seq aligner. Bioinformatics. 2013; 29(1):15–21.

535   35.   Anders S, Reyes A, Huber W. Detecting differential usage of exons from RNA-seq data.
536   Genome Res. 2012; 22(10):2008–17.

537   36.   Bedre R. reneshbedre/bioinfokit: Bioinformatics data analysis and visualization toolkit.
538   2020 [cited 2020]; . Available from:
539   https://doi.org/10.5281/zenodo.3965241#.X1p62G7zZyE.mendeley

540   37.   Karimzadeh M, Ernst C, Kundaje A, Hoffman MM. Umap and Bismap: quantifying genome
541   and methylome mappability. Nucleic Acids Res. 2018; 46(20):e120.

542   38.   Wu J, Anczukow O, Krainer AR, Zhang MQ, Zhang C. OLego: fast and sensitive mapping of
543   spliced mRNA-Seq reads using small seeds. Nucleic Acids Res. 2013; 41(10):5149–63.

544   39.   Li YI, Knowles DA, Humphrey J, Barbeira AN, Dickinson SP, Im HK, et al. Annotation-free

545   quantification of RNA splicing using LeafCutter. Nat Genet. 2018; 50(1):151–8.

546   40.   An J-Y, Lin K, Zhu L, Werling DM, Dong S, Brand H, et al. Genome-wide de novo risk score
547   implicates promoter variation in autism spectrum disorder. Science. 2018;
548   362(6420):eaat6576.

549   41.   Ongen H, Buil A, Brown AA, Dermitzakis ET, Delaneau O. Fast and efficient QTL mapper
550   for thousands of molecular phenotypes. Bioinformatics. 2016; 32(10):1479–85.

551   42.   Benjamini Y, Hochberg Y. Controlling the False Discovery Rate: A Practical and Powerful
552   Approach to Multiple Testing. J R Stat Soc Ser B. 1995; 57(1):289–300.

553   43.   Nowakowski TJ, Bhaduri A, Pollen AA, Alvarado B, Mostajo-Radji MA, Di Lullo E, et al.
554   Spatiotemporal gene expression trajectories reveal developmental hierarchies of the
555   human cortex. Science [Internet]. 2017; 358(6368):1318–23. Available from:
556   http://www.sciencemag.org/lookup/doi/10.1126/science.aap8809

557   44.   Li M, Santpere G, Kawasawa YI, Evgrafov O V., Gulden FO, Pochareddy S, et al. Integrative
558   functional genomic analysis of human brain development and neuropsychiatric risks.
559   Science. 2018; 362(6420).

560   45.   Tang L, Lu X, Tao Y, Zheng J, Zhao P, Li K, et al. SCN1A rs3812718 polymorphism and
561   susceptibility to epilepsy with febrile seizures: a meta-analysis. Gene. 2014; 533(1):26–
562   31.

563   46.   Wang ZJ, Chen J, Chen HL, Zhang LY, Xu D, Jiang WT. Association between SCN1A
564   polymorphism rs3812718 and valproic acid resistance in epilepsy children: a case-
565   control study and meta-analysis. Biosci Rep. 2018; 38(6).

566   47.   The International League Against Epilepsy Consortium on Complex Epilepsies. Genome-
567   wide mega-analysis identifies 16 loci and highlights diverse biological mechanisms in the
568   common epilepsies. Nat Commun. 2018; 9(1):5269.

569   48.   Heinzen EL, Yoon W, Tate SK, Sen A, Wood NW, Sisodiya SM, et al. Nova2 interacts with a
570   Cis-acting polymorphism to influence the proportions of drug-responsive splice variants
571   of SCN1A. Am J Hum Genet. 2007; 80(5):876–83.

572   49.   GTEx Consortium. Human genomics. The Genotype-Tissue Expression (GTEx) pilot
573   analysis: multitissue gene regulation in humans. Science [Internet]. 2015;
574   348(6235):648–60. Available from: http://www.ncbi.nlm.nih.gov/pubmed/25954001

575   50.   Jaganathan K, Kyriazopoulou Panagiotopoulou S, McRae JFJF, Darbandi SFSF, Knowles D,
576   Li YIYI, et al. Predicting Splicing from Primary Sequence with Deep Learning. Cell
577   [Internet]. 2019; 0(0):1–14. Available from:
578   https://linkinghub.elsevier.com/retrieve/pii/S0092867418316295

579   51.   Kim J, Hu C, Moufawad El Achkar C, Black LE, Douville J, Larson A, et al. Patient-
580   Customized Oligonucleotide Therapy for a Rare Genetic Disease. N Engl J Med. 2019;
581   381(17):1644–52.

582   52.   Finkel RS, Mercuri E, Darras BT, Connolly AM, Kuntz NL, Kirschner J, et al. Nusinersen

583   versus Sham Control in Infantile-Onset Spinal Muscular Atrophy. N Engl J Med [Internet].
584   2017/11/02. 2017; 377(18):1723–32. Available from:
585   https://www.ncbi.nlm.nih.gov/pubmed/29091570

586   53.   Berkovic SF, Grinton B, Dixon-Salazar T, Laughlin BL, Lubbers L, Milder J, et al. De novo
587   variants in the alternative exon 5 of SCN8A cause epileptic encephalopathy. Genet Med.
588   2018; 20(2):275–81.

589   54.   Sanders SJ, Campbell AJ, Cottrell JR, Moller RS, Wagner FF, Auldridge AL, et al. Progress in
590   Understanding and Treating SCN2A-Mediated Disorders. Vol. 41, Trends in
591   Neurosciences. 2018. p. 442–56.

592   55.   Xu R, Thomas EA, Jenkins M, Gazina E V., Chiu C, Heron SE, et al. A childhood epilepsy
593   mutation reveals a role for developmentally regulated splicing of a sodium channel. Mol
594   Cell Neurosci. 2007; 35(2):292–301.

595   56.   Anvar SY, Allard G, Tseng E, Sheynkman GM, de Klerk E, Vermaat M, et al. Full-length
596   mRNA sequencing uncovers a widespread coupling between transcription initiation and
597   mRNA processing. Genome Biol. 2018; 19(1):1–18.

598   57.   Clark MB, Wrzesinski T, Garcia AB, Hall NAL, Kleinman JE, Hyde T, et al. Long-read
599   sequencing reveals the complex splicing profile of the psychiatric risk gene CACNA1C in
600   human brain. Mol Psychiatry [Internet]. 2020; 25(1):37–47. Available from:
601   http://dx.doi.org/10.1038/s41380-019-0583-1

602   58.   Gupta I, Collier PG, Haase B, Mahfouz A, Joglekar A, Floyd T, et al. Single-cell isoform RNA
603   sequencing characterizes isoforms in thousands of cerebellar cells. Nat Biotechnol. 2018;
604   .

605   59.   Quinlan AR, Hall IM. BEDTools: a flexible suite of utilities for comparing genomic
606   features. Bioinformatics. 2010; 26(6):841–2.

607   60.   Patro R, Duggal G, Love MI, Irizarry RA, Kingsford C. Salmon provides fast and bias-aware
608   quantification of transcript expression. Nat Methods. 2017; 14(4):417–9.

609

610